

NLTE analysis of Co I/Co II lines in spectra of cool stars with new laboratory hyperfine splitting constants [★]

Maria Bergemann^{1,3,†}, Juliet C. Pickering^{2,‡}, and Thomas Gehren^{3,§}

¹Max-Planck Institute for Astrophysics, Karl-Schwarzschild Str. 1, 85741, Garching, Germany

²Physics Department, Blackett Laboratory, Imperial College, London SW7 2BZ, UK

³University Observatory, Ludwig-Maximilian University, Scheinerstr. 1, 81679 Munich, Germany

Accepted Date. Received Date; in original Date

ABSTRACT

The analysis of stellar abundances for odd-Z Fe-peak elements requires accurate NLTE modelling of spectral lines fully taking into account the hyperfine structure splitting (HFS) of lines. Here, we investigate the statistical equilibrium of Co in the atmospheres of cool stars, and the influence of NLTE and HFS on the formation of Co lines and abundances. Significant departures from LTE level populations are found for Co I, also number densities of excited states in Co II differ from LTE at low metallicity. The NLTE level populations are used to determine the abundance of Co in solar photosphere, $\log \epsilon = 4.95 \pm 0.04$ dex, which is in agreement with that in C I meteorites within the combined uncertainties. The spectral lines of Co I were calculated using the results of recent measurements of hyperfine interaction constants by UV Fourier transform spectrometry. For Co II, the first laboratory measurements of hyperfine structure splitting *A* and *B* factors were performed. These highly accurate *A* factor measurements (errors of the order of 3-7%) allow, for the first time, reliable modelling of Co II lines in the solar and stellar spectra and, thus, a test of the Co I/Co II ionization equilibrium in stellar atmospheres. A differential abundance analysis of Co is carried out for 18 stars in the metallicity range $-3.12 < [\text{Fe}/\text{H}] < 0$. The abundances are derived by method of spectrum synthesis. At low $[\text{Fe}/\text{H}]$, NLTE abundance corrections for Co I lines are as large as $+0.6 \dots +0.8$ dex. Thus, LTE abundances of Co in metal-poor stars are severely underestimated. The stellar NLTE abundances determined from the single UV line of Co II are lower by $\sim 0.5 - 0.6$ dex. The discrepancy might be attributed to possible blends that have not been accounted for in the solar Co II line and its erroneous oscillator strength. The increasing $[\text{Co}/\text{Fe}]$ trend in metal-poor stars, as calculated from the Co I lines under NLTE, can be explained if Co is overproduced relative to Fe in massive stars. The models of galactic chemical evolution are wholly inadequate to describe this trend suggesting that the problem is in SN yields.

Key words: Atomic data – Line: profiles – Line: formation – Stars: abundances

1 INTRODUCTION

Cobalt is one of the most intriguing elements in studies of galactic chemical evolution. There is neither an agreement on the overall abundance trend of Co in the halo and thin/thick disk, nor a generally accepted scenario for the nucleosynthetic production of cobalt.

Several investigations of Co abundances have been done in various metallicity regimes and stellar populations. All of these abundance investigations were based on Co I lines and local thermodynamic equilibrium (LTE) for the line formation. According to the results of Gratton & Sneden (1991), Co follows the depletion of

Fe down to $[\text{Fe}/\text{H}] \approx -2.5$. At lower metallicities, McWilliam et al. (1995) observe a strong increase of cobalt abundance with respect to iron by ~ 0.5 dex. Del Peloso et al. (2005) obtained a different trend for $[\text{Co}/\text{Fe}]$, characterized by a steady increase towards supersolar ratios of $\sim +0.2$ from $[\text{Fe}/\text{H}] = 0$ to -0.8 . An excess of cobalt with respect to iron at $-4 \leq [\text{Fe}/\text{H}] \leq -2.5$ was reported by Lai et al. (2008), Cayrel et al. (2004), and Ryan et al. (1991). Reddy et al. (2003, 2006) find supersolar and mildly subsolar Co abundances for the thick and thin disk stars, respectively.

The increasing $[\text{Co}/\text{Fe}]$ ratio with decreasing metallicity was attributed to the Co production in both types of supernovae (SNe) but with uncertain relative contributions (Del Peloso et al. 2005). However, this is hard to understand from the point of view of stellar nucleosynthesis. Cobalt is an odd-Z element of the Fe-group and is produced in α -rich freeze-out in SNe. Thus, its abundance must be sensitive to the explosion entropy and neutron excess available to

[★] Based on observations collected at the European Southern Observatory, Chile, 67.D-0086A, and the Calar Alto Observatory, Spain.

[†] E-mail: mbergema@mpa-garching.mpg.de (MB)

[‡] E-mail: j.pickering@imperial.ac.uk (JCP)

[§] E-mail: gehren@usm.lmu.de (TG)

the progenitor star in the explosive Si-burning phase. The neutron enrichment is determined by the initial metal content of a star and by the previous hydrostatic burning stages. Hence, in metal-poor environments we expect to see an *odd-even effect* characterized by a general suppression of the stable odd- Z nuclei relative to their stable even- Z neighbours (Burbidge et al. 1957). Still, this effect is in conflict with the increasing $[\text{Co}/\text{Fe}]$ trend in metal-poor stars.

Thus far, any attempt to describe the abundances of Co within the framework of explosive nucleosynthesis in SNe failed. Models of galactic chemical evolution (GCE), which use standard metallicity-dependent prescriptions for Co production in SNe II (Woosley & Weaver 1995) and SNe Ia (Nomoto et al. 1984; Iwamoto et al. 1999) predict a decreasing or nearly flat $[\text{Co}/\text{Fe}]$ trend (Timmes et al. 1995; Samland 1998; Goswami & Prantzos 2000). Models with metallicity-independent SN yields give only a qualitatively similar behaviour, however large discrepancies with spectroscopic abundances are seen either for the thick disk (Goswami & Prantzos 2000) or for the halo (François et al. 2004).

There are several explanations for the disagreement between observed Co trends and predictions of chemical evolution models. Deficiencies of the latter are hidden among others in the assumed shape of the initial mass function (IMF). As shown by Wang & Silk (1993), the shape of the IMF introduces a factor of 2 in uncertainty to the absolute yield value of an element. The physics of supernova explosions is still poorly understood (Thielemann et al. 2007), hence theoretical stellar yields for Co may be erroneous. It is also important to note that the majority of GCE models assume a single gas phase for the galactic ISM, and only a few consider multiphase ISM (e.g. Schönrich & Binney 2009) that is crucial for a physically accurate description of the galactic chemo-dynamical evolution.

On the other hand, a close examination of the 'observed' Co abundances in the Sun and metal-poor stars reveals that all of them rely on several coarse assumptions: LTE in the line formation, static 1D atmospheric models, and, often, neglect of hyperfine structure splitting (HFS) of lines. The errors in abundances caused by these approximations are hard to predict, especially because effects of NLTE and temperature inhomogeneities are not independent (Asplund 2005). Iron is the only representative of the Fe-group for which calculations of 1.5D NLTE line formation with 3D convective model atmospheres have been performed. NLTE analyses with 1D model atmospheres exist for a number of elements, specifically for Fe (see Korn et al. 2003, and references therein), Sc (Zhang et al. 2008), and Mn (Bergemann & Gehren 2008). These and other studies prove that the NLTE abundance corrections can be significant at low gravities and/or metallicities. Due to the over-ionization, NLTE abundances of Mn in metal-poor stars are larger by $+0.1 \dots +0.6$ dex than those computed under LTE.

Knowledge of hyperfine structure (HFS) in odd- Z iron-group elements is essential in calculations of line formation and abundances. The reason is that HFS is not merely a line broadening mechanism; it modifies absorption over the entire line profile, especially for strong and saturated lines. Thus, neglect of HFS results in wavelength shifts, incorrectly determined damping parameters, and erroneous abundances (this last issue is addressed in Holweger & Oertel 1971; Prochaska & McWilliam 2000; Del Peloso et al. 2005). In a strictly *differential* analysis of stars with respect to the Sun, which is usually preferred in order to minimize other deficiencies of the stellar atmosphere modelling, neglect of HFS for the reference solar spectral lines may lead to systematically *underestimated* abundances in metal-poor stars. The accuracy of the adopted HFS factors is also important, as we will show in this paper. At present, high resolution measurements of

HFS over a wide spectral range are possible with high resolution Fourier transform spectrometry (FTS). For example, an analysis of Co I was undertaken using over one thousand line profiles acquired with the FT spectrometer at Imperial College, and yielded HFS A splitting factors for 297 energy levels, almost all known Co I energy levels (Pickering 1996).

In this paper, we investigate the excitation-ionization equilibrium of Co in stellar atmospheres and predict what errors in abundance calculations occur when NLTE effects and hyperfine splitting of lines are neglected. Given the particular importance of HFS in this context, we have measured hyperfine splitting of Co II energy levels using the technique of FTS. We analyze the abundance of Co in the Sun, and compare it with that of meteorites to ascertain the reason for the discrepancies. Furthermore, we compute the NLTE abundances for a sample of 18 stars, which belong to the thin and thick disk, and the halo. The evolution of abundance ratios in the Galaxy and some implications for the Fe-peak element nucleosynthesis are discussed.

2 MEASUREMENTS OF THE HYPERFINE STRUCTURE OF CO II LEVELS

2.1 Simple Theory

For atoms with non zero nuclear spin I the fine structure levels undergo splitting because of the hyperfine interaction between the nucleus and the electrons. In the absence of perturbations the energy of the hyperfine structure multiplets is given (Kopfermann 1958) by:

$$W_F = W_J + \frac{1}{2}AK + B \frac{(3/4)K(K+1) - J(J+1)I(I+1)}{2I(2I-1)J(2J-1)} \quad (1)$$

where W_J is the energy of the fine structure level of quantum number J , A and B are the magnetic dipole and the electric quadrupole hyperfine interaction constants respectively, and K is defined as

$$K = F(F+1) - J(J+1) - I(I+1)$$

in which F is the quantum number associated with the total angular momentum of the atom,

$$F = I + J; \quad I + J - 1; \quad \dots; \quad |I - J|$$

The selection rules which govern the hyperfine transitions are: $\Delta F = 0; \pm 1$ but not $F = 0 \leftrightarrow F = 0$

In addition there are intensity rules (Kuhn 1962): within a hyperfine multiplet the ratio of the sums of the intensities of all transitions from two states with quantum numbers F and F' are in the ratio of their statistical weights $(2F+1):(2F'+1)$.

This simple theory was used in the fitting of HFS of the Co II transitions in this work. For Co, nuclear spin $I = 7/2$. No perturbations were evident.

2.2 Experimental Details

The spectra used in this work were obtained as part of an extensive measurement of the Co II spectrum, by FTS with cobalt-neon and cobalt-argon hollow cathode lamps as sources, in the wavelength region $1420 - 33000 \text{ \AA}$ ($70422 - 3000 \text{ cm}^{-1}$), resulting in a doubling of the number of classified lines, over 200 new energy levels (Pickering et al. 1998; Pickering 1998a,b), and new calculations of Co II oscillator strengths (Raassen et al. 1998). These papers give identified line lists, including the centre-of-gravity (COG)

wavenumber and intensity of each transition, together with tables of energy levels. Most of the Co II lines exhibit broadening due to hyperfine structure. The spectra used for this HFS study were acquired in the visible-UV region with the vis-VUV Fourier transform (FT) spectrometer at Imperial College, with resolution 0.037 cm^{-1} (0.006 \AA) in the visible, 0.05 cm^{-1} (0.003 \AA) in the UV, the individual line components being limited by their Doppler widths alone. The light source was a water-cooled hollow cathode lamp run in either Ar at 1 mbar or Ne at 2 – 3 mbar, with currents of 600 – 700 mA, using a pure cobalt cathode.

2.3 Hyperfine Structure Analysis

The determination of the A and B factors for the Co II energy levels presented in this paper was carried out using a HFS analysis subroutine in the spectrum analysis program Xgremlin (Nave et al. 1997). The input information comprises the I -value, the J -values of both levels, the known intensity ratios of the transition components (Kuhn 1962), the widths of the components (having Gaussian and Lorentzian contributions), the COG of the pattern and, where possible (see below) an A factor for one of the two levels. A large scale study of Co II HFS is ongoing at Imperial College, and here we report a detailed investigation of A factors for the $3d^7(^4P)4s \ a^5P_{3,2,1}$ levels and for three of the four $3d^7(^4F)4p \ z^5D_{4,3,1}^o$ levels, with immediate application in this work.

It was not possible to determine the electric quadrupole hyperfine interaction constant B to great accuracy, because the contribution of the last term in Eq. 1 was so small, but B factors are estimated. The analysis was particularly challenging because no previous measurements existed, but with a comprehensive study we were able to set a starting point for the fits of line profiles in cases where an initial guess at the A factors could be made from a characteristic line profile pattern. For example, when one of the A factors of the levels involved in a transition is an order of magnitude greater than the other A factor, the line profile has a characteristic “flag” pattern (examples shown in Pickering 1996). These A factors could then be used to find A factors of other levels using different transitions, building up the number of known A factors.

In general, for each level studied the HFS A factor was determined from the analysis of line profiles for between 3 and 6 different transitions, however in the case of the even levels reported here between 7 and 13 line profiles were fitted.

The resolution of the FT spectrometer is such that the line widths are limited solely by the Doppler widths and so, depending on the size of the A factors, the overall pattern is usually well resolved into individual components in the IR region, but only partly so in the UV. However, even where a set of line profiles did not appear to be resolved into individual components, the fitting still gave consistent sets of A factors.

The high number of fitted lines, the fact that the A factors were relatively large in magnitude compared to those of higher lying odd levels, and good signal-to-noise ratio of studied lines gave reliable A factors for the $a^5P_{3,2,1}$ levels with uncertainties ranging between 3 – 7 %. However, fitting of line profiles to find the A factors for the four odd z^5D^o levels was less reliable because of the smaller value of the A factor, resulting in almost no visible structure in the line profile. A factors for these odd levels should be considered to be *estimates*.

The values determined for the A and B splitting factors are listed in Table 1, and they are the weighted average values from the line fits with weighting dependent on the signal-to-noise ratio of the transitions of the individual line fits (Blackwell-Whitehead et al.

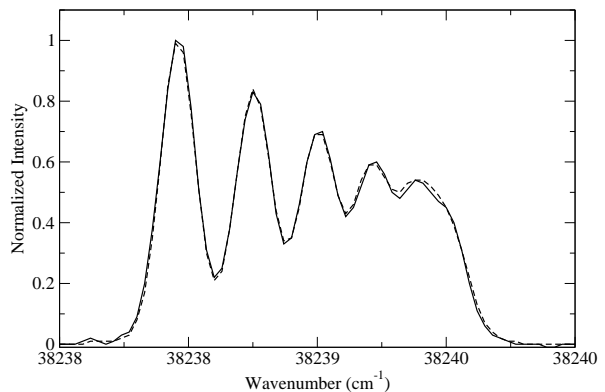


Figure 1. An example of an observed (heavier trace in plot) and fitted (dashed trace) line profile, for a Co II transition recorded by FTS: $(38238.965 \text{ cm}^{-1}) \ 2614.3530 \text{ \AA}$ transition, $3d^7(^4P)4s \ a^5P_3 - 3d^7(^4P)4s \ z^5D_2^o$.

Table 1. Hyperfine structure interaction constants A and B for selected energy levels of Co II. N denotes the number of profiles fitted.

Configuration	Term	J	Energy cm^{-1}	A mK	err mK	B mK	err mK	N	
$3d^7(^4P)4s$	a^5P	3	17771.506	40.0	3	-20	30	10	
		2	18031.426	49.9	1.5	20	30	13	
		1	18338.639	60.0	2	2	5	7	
$3d^7(^4F)4p$	z^5D^o	4	46320.829	9.0	2	10	50	3	
		3	47039.102	8.0	20	-	-	1	
		2	47537.362 ¹						
		1	47848.778 ²	<10	-	-	-	-	

Note: ¹ transitions could not be reliably fitted as part of this work to date,

² transitions involving $z^5D_1^o$ were observed to be narrow, consistent with $A < 10$ mK, but fitting was unreliable, so an upper limit of the A factor alone is given here as a guide.

2005). The uncertainties listed in Table 1 are estimated from the range of values of each particular A factor, from the standard deviation. In Table 1 the first four columns give, for each level investigated, the configuration, term designation, J -value and energy reported in Pickering et al. (1998). The fifth and sixth columns give the A factor and its uncertainty in mK ($1\text{mK}=0.001\text{cm}^{-1}$) determined in this work. The next column lists, where appropriate, approximate values of B factors and their uncertainty. The final column gives the number of line profiles fitted in the process of finding that A factor. An example of a fitted line profile used in this work is shown in Fig. 1.

3 NLTE LINE FORMATION

3.1 The methods, model atmospheres, and stellar parameters

The statistical equilibrium (SE) calculations for Co are carried out with the DETAIL code (Butler & Giddings 1985), with the radiative transfer based on the method of accelerated lambda iteration.

Spectrum synthesis is performed using the SIU code written

by J. Reetz. The profiles of Co I and Co II lines are computed with NLTE atomic level populations from SE calculations. Radiation damping is derived from the oscillator strengths of transitions. Damping due to quadratic Stark and van der Waals effects follows the expressions given by Unsöld (1955). However, the atomic interaction parameter C_6 is calculated using the line half-widths due to elastic collisions with H I computed from the theory of Anstee & O'Mara (1995). The $\log C_6$ values and other parameters for each Co line investigated in this work are given in Table 2.

The hyperfine structure of lines is taken into account by superposing individually synthesised HFS components. Relative intensities of the components are calculated according to the tables of White & Eliason (1933). Wavelengths are computed using the laboratory data for A and B factors. HFS data for all Co I levels are taken from Pickering (1996). For the levels of Co II, we use our new values as described in Sect. 2. The A and B factors are given in the Table A1 available online.

Abundances are determined by fitting the synthetic lines to the observed line profiles. The analysis of stars is *strictly differential*¹ relative to the Sun, i.e. any abundance estimate derived from a single line in a spectrum of a metal-poor star is referred to that from the corresponding solar line. This excludes the use of oscillator strengths in calculation of stellar [Co/Fe] ratios.

All computations, including determinations of stellar parameters, are based on the model atmospheres computed with the MAFAGS code. These are static 1D plane-parallel models with line blanketing computed with opacity distribution functions of Kurucz (1992). Convection is taken into account using the mixing-length theory (Böhm-Vitense 1958) with the mixing length parameter $\alpha = 0.5$. Some examples and tests of MAFAGS-ODF models are given in Grupp (2004). Note that due to physical limitations of such classical 1D LTE models, our analysis is restricted to turnoff stars. Only one giant, HD 122563, is included for purposes of comparison with other studies.

Basic parameters for the program stars were adopted from Fuhrmann (2004), Gehren et al. (2004, 2006), and Mashonkina et al. (2008). These analyses make use of the following methods. The effective temperatures were derived by fitting the observed H α and H β profiles under LTE assumption. The surface gravities were calculated using parallaxes π measured by *Hipparchos* (ESA 1997) and bolometric corrections were taken BC from Alonso et al. (1995). Masses were determined from the tracks of VandenBerg et al. (2000) by interpolating in the $M_{\text{bol}} - T_{\text{eff}}$ diagram. The iron abundances and microturbulent velocities were obtained from Fe II line profile fitting in LTE. For the thick disk and halo stars, the abundances of α -elements are enhanced by ~ 0.4 dex. The population identification is based on stellar kinematic properties, ages, and abundance ratios [Al/Mg]. All stellar parameters are listed in Table 3.

3.2 Atomic model

The model of the Co atom is constructed as follows. The number of levels and transitions is 246 and 6027 for Co I, and 165 and 2539 for Co II. The energy separation of the highest excited level from the continuum is 0.4 eV for Co I and ~ 3 eV

Table 2. Lines of Co I and Co II selected for solar and stellar abundance calculations. N denotes a number of HFS components for a line, and the multiplet is specified in the 2-d column. E_{low} is the excitation energy of the lower level of a transition. W_λ refers to the line equivalent width. An asterisk in the wavelength entry refers to the lines, which are not used in determination of the solar Co abundance due to blending or inaccurate $\log gf$'s.

λ [Å]	Mult.	N	E_{low} [eV]	Lower level	Upper level	W_λ [mÅ]	$\log gf^a$	$\log C_6$
Co I								
3845.470*	34	4	0.92	$a^2F_{7/2}$	$y^2G_{9/2}^o$	120	0.01 2	-31.5
3957.930*	18	3	0.58	$b^4F_{5/2}$	$z^4D_{5/2}^o$	60	-2.07 2	-31.7
4020.905	16	6	0.43	$b^4F_{9/2}$	$z^4F_{9/2}^o$	76	-2.04 1	-31.8
4066.360*	30	3	0.92	$a^2F_{7/2}$	$y^4D_{7/2}^o$	59	-1.60 1	-31.6
4110.530	29	6	1.05	$a^2F_{5/2}$	$z^2F_{5/2}^o$	95	-1.08 2	-31.6
4121.320	28	4	0.92	$a^2F_{7/2}$	$z^2G_{9/2}^o$	131	-0.30 1	-31.7
4792.862*	158	6	3.25	$z^6G_{7/2}^o$	$e^6F_{5/2}$	34	-0.07 3	-30.5
4813.480*	158	7	3.22	$z^6G_{9/2}^o$	$e^6F_{7/2}$	44	0.05 3	-30.5
4867.870*	158	10	3.17	$z^6G_{11/2}^o$	$e^6F_{9/2}$	60	0.23 3	-30.6
5212.691	170	9	3.51	$z^4F_{9/2}^o$	$f^4F_{9/2}$	25	-0.11 2	-30.5
5280.631	172	8	3.63	$z^4G_{9/2}^o$	$f^4F_{7/2}$	20	-0.03 2	-30.4
5301.047	39	5	1.71	$a^4P_{5/2}$	$y^4D_{5/2}^o$	21	-1.94 1	-31.5
5331.460	39	5	1.78	$a^4P_{1/2}$	$y^4D_{3/2}^o$	17	-1.99 1	-31.5
5352.049	172	9	3.58	$z^4G_{11/2}^o$	$f^4F_{9/2}$	26	0.06 2	-30.5
5369.590*	39	4	1.74	$a^4P_{3/2}$	$y^4D_{5/2}^o$	44	-1.59 1	-31.5
5483.340	39	7	1.71	$a^4P_{5/2}$	$y^4D_{7/2}^o$	51	-1.41 1	-31.5
5647.234	112	6	2.28	$a^2P_{3/2}$	$y^2D_{5/2}^o$	14	-1.56 2	-31.4
6189.000*	37	9	1.71	$a^4P_{5/2}$	$z^4D_{5/2}^o$	11	-2.45 2	-31.7
6454.990	174	8	3.13	$z^4D_{7/2}^o$	$e^6F_{9/2}$	15	-0.25 2	-30.4
6814.950*	54	5	1.96	$b^4P_{3/2}$	$z^4D_{3/2}^o$	19	-1.90 2	-31.7
7417.380*	89	8	2.04	$a^2D_{3/2}$	$z^4D_{5/2}^o$	11	-2.07 2	-31.7
7712.661*	126	8	2.04	$b^2P_{3/2}$	$z^2D_{5/2}^o$	10	-1.57 2	-31.5
Co II								
3501.730	2	8	2.19	a^5P_3	$z^5D_4^o$	86	-1.22 4	-32.2

^a References: (1) Nitz et al. (1999); (2) Cardon et al. (1982); (3) Kurucz & Peytremann (1996); (4) Raassen et al. (1998)

for Co II. Energies of levels and wavelengths of transitions are taken from Pickering & Thorne (1996) and Pickering et al. (1998). The oscillator strengths are adopted from the Kurucz' database (Kurucz & Bell 1995), which includes laboratory measurements and data calculated using scaled Thomas-Fermi-Dirac radial wavefunctions. A complete Grotrian diagram for Co is available online.

Hyperfine splitting of the levels was not included in the SE calculations, since *relative* populations of HFS components are thermal. Moreover, for the uppermost terms above 6.3 eV in Co I the fine structure is not maintained. These terms are represented by a single level with a weighted mean of statistical weights and ionization frequencies of their fine structure levels. The transitions between two combined levels are also grouped, and the oscillator strength of a resulting line is the average of $\log gf$'s weighted according to the appropriate lower-level statistical weights.

Since no quantum-mechanical calculations of photoionization for Co I and Co II are available, hydrogenic approximation is used. The cross-sections are computed from the formula of Kramer (Menzel & Pekeris 1935) corrected for the ion charge (see, e.g., Rutten 2003) and using the *effective* hydrogen-like main quantum number. For cross-sections of collisional ionization, we use the formula of Seaton (1962). The rates of allowed and forbidden bound-

¹ The differential element abundance in a metal-poor star is given by

$$[E/H] = \log(gf\epsilon)_* - \log(gf\epsilon)_\odot$$

Table 3. Stellar parameters and their estimated errors for the selected sample. In the *Ref* column, the sources of adopted stellar parameters are given.

Object	HIP	Instr.	T_{eff} [K]	$\log g$	ξ_t [km/s]	[Fe/H]	[Mg/Fe]	π/σ_π	Population	Ref. ^a	N_{Co}	[Co/Fe] NLTE	LTE
HD 19445	14594	FOCES	5985 ± 80	4.39 ± 0.05	1.5	-1.96	0.38	22.7	Halo	1	1	0.64	0.08
HD 25329	18915	FOCES	4800 ± 80	4.66 ± 0.08	0.6	-1.84	0.42	50.1	Thick Disk?	4	1	-0.02	-0.72
HD 29907	21609	UVES	5573 ± 100	4.59 ± 0.09	0.9	-1.60	0.43	17.3	Halo?	2	2	0.66 ± 0.06	0.19 ± 0.05
HD 34328	24316	UVES	5955 ± 70	4.47 ± 0.07	1.3	-1.66	0.42	14.4	Halo	2	3	0.67 ± 0.01	0.11 ± 0.16
HD 61421	37279	UVES	6510 ± 100	3.96 ± 0.05	1.8	-0.03	0.0	324.9	Thin Disk	5	8	-0.09 ± 0.07	-0.15 ± 0.1
HD 84937	48152	UVES	6346 ± 100	4.00 ± 0.08	1.8	-2.16	0.32	11.7	Halo	1	3	0.66 ± 0.03	0.18 ± 0.01
HD 102200	57360	UVES	6120 ± 90	4.17 ± 0.09	1.4	-1.28	0.34	10.5	Halo	2	3	0.51 ± 0.06	0.03 ± 0.11
HD 103095	57939	FOCES	5110 ± 100	4.69 ± 0.10	1.0	-1.35	0.26	140.0	Halo	1	1	-0.01	-0.11
BD-4°3208	59109	UVES	6310 ± 60	3.98 ± 0.21	1.5	-2.23	0.34	3.7	Halo	2	2	0.71 ± 0.08	0.13 ± 0.01
HD 122196	68464	UVES	5957 ± 80	3.84 ± 0.11	1.7	-1.78	0.24	7.4	Halo	2	2	0.52 ± 0.02	-0.12 ± 0.06
HD 122563	68594	UVES	4600 ± 120	1.50 ± 0.20	1.9	-2.51	0.45	5.2	Halo	3	3	0.57 ± 0.02	-0.07 ± 0.06
HD 134169	74079	FOCES	5930 ± 200	3.98 ± 0.1	1.8	-0.86	0.53	15.1	Thick disk	1	3	0.45 ± 0.02	0.18 ± 0.14
HD 148816	80837	FOCES	5880 ± 200	4.07 ± 0.07	1.2	-0.78	0.36	27	Thick disk	2	6	0.38 ± 0.03	0.19 ± 0.06
HD 184448	96077	FOCES	5765 ± 200	4.16 ± 0.07	1.2	-0.43	0.47	30.4	Thick disk	2	11	0.34 ± 0.04	0.27 ± 0.03
HD 140283	76976	UVES	5773 ± 60	3.66 ± 0.05	1.5	-2.38	0.43	18.0	Halo	2	3	0.85 ± 0.02	0.14 ± 0.01
G 20-8	86443	FOCES	6115 ± 80	4.20 ± 0.20	1.5	-2.19	0.45	5.1	Halo	1	2	0.76 ± 0.06	0.28 ± 0.15
G 64-12	66673	UVES	6407 ± 80	4.20 ± 0.20	2.3	-3.12	0.33	1.3	Halo	1	1	0.8 ± 0.1	0.19 ± 0.1
HD 200580	103987	FOCES	5940 ± 80	3.96 ± 0.06	1.4	-0.82	0.46	13.8	Thick Disk	2	2	0.38 ± 0.04	0.12 ± 0.1

^a References: (1) Gehren et al. (2006); (2) Gehren et al. (2004); (3) Mashonkina et al. (2008); (4) Fuhrmann (2004); (5) Korn et al. (2003)

bound transitions due to collisions with electrons are calculated using the formulae of van Regemorter (1962) and Allen (1973), respectively.

The rates of bound-bound and bound-free transitions due to inelastic collisions with H I atoms are computed from the formula of Drawin (1969) in the version of Steenbock & Holweger (1984) and are multiplied by a scaling factor $S_{\text{H}} = 0.05$. This value gave the smallest fitted-abundance spread in our previous work on SE of Mn in stellar atmospheres (Bergemann & Gehren 2007, 2008). Most abundance analyses favour similar small values of S_{H} (Mashonkina 1996; Abia & Mashonkina 2004; Sundqvist et al. 2008; Shi et al. 2008). To the best of our knowledge, there are only a few indications in the literature that S_{H} is *larger* than unity (Gratton et al. 1999; Korn et al. 2003). Unfortunately, these cases refer to the most prominent member of the Fe-group, iron.

In subsequent sections, we study the influence of photoionization cross-sections and inelastic collisions with hydrogen on populations of atomic levels in Co. However, it should be kept in mind that values for cross-sections have only order-of-magnitude accuracy.

4 RESULTS

4.1 Statistical equilibrium of Co

To discuss the excitation-ionization equilibrium of Co in stellar atmospheres, we use the notation of the *departure coefficient* b_i , which is defined as $b_i = N_i^{\text{NLTE}}/N_i^{\text{LTE}}$ with N_i the number density of atoms in the level i . The b_i -factors as a function of optical depth at 500 nm are presented in Fig. 2 for the solar model atmosphere and several stellar models from the grid. A few selected levels, typical for their depth dependence, are indicated by heavier black traces;

the remaining bulk of the Co I and Co II levels are indicated by grey lines.

4.1.1 The Sun

Fig. 2a shows the departure coefficients, calculated with our *reference* model of Co for the Sun. The overall underpopulation of all Co I levels is due to the *overionization* mainly from the levels of 2–3 eV excitation, e.g. z^2G^o with threshold wavelength 3151 Å. The Co I ground state is not subject to strong overionization. But its separation from the first metastable level is only 0.4 eV, which favours a very efficient collisional interaction. Strong collisional and radiative coupling also persists between other Co I levels, because the total number of transitions in Co I is very large. Thus, the distribution of b -factors up to $\log \tau_{5000} \sim -2$ has a very regular structure, with levels of ever decreasing energy gap from the continuum showing smaller deviations of b_i from unity.

In the higher layers, spontaneous transitions in strong lines of Co I slightly modify this simple pattern. At $\log \tau_{5000} \leq -1.5$, the medium becomes transparent to the radiation in transitions between the low metastable levels and the levels of odd doublet and quartet term systems with ~ 4 eV excitation energy, that leads to a depletion of the upper levels. One such transition, $a^2F_{7/2} \rightarrow z^2G_{9/2}^o$, is of particular interest, because the corresponding spectral line 4121 Å is the only observable line of Co I in our spectra of very metal-poor stars.

A large number of strong transitions with UV wavelengths in Co I connect the low levels with 0–3 eV and the levels with 5–6 eV excitation energies E_i . Hence, at depths with $-1 < \log \tau_{5000} < 0.2$ there is also *overexcitation* of the upper levels. This maintains nearly constant b_i of upper levels at $-1 < \log \tau_{5000} < 0$, in spite of increasing overionization (e.g. level e^6G in Fig. 2a). This process

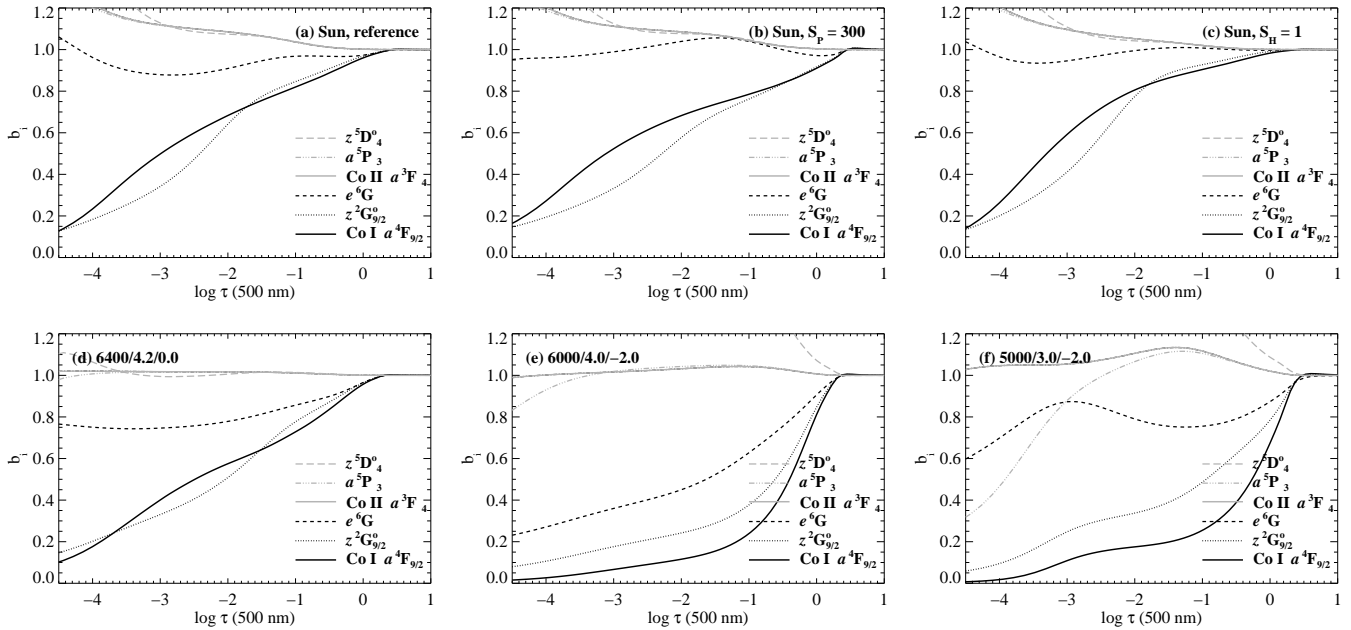


Figure 2. Departure coefficients b_i of selected Co I and Co II levels for the solar model and for several stellar models from the grid.

barely affects populations of the lower levels due to the small Boltzmann factor, and dominance of photoionization from these levels.

The majority of the uppermost levels with $E_i > 6.5$ eV are underpopulated relative to the continuum. They interact much stronger radiatively with the low levels and with each other by means of collisions than with the Co II ground state, a^3F_4 . Only for a few highest levels, with threshold ionization energies similar to the mean kinetic energy of the electrons in the solar atmosphere, does the collisional coupling to the a^3F_4 level prevail. Thus, they are in thermal equilibrium with a^3F_4 .

The ground state of Co II is also affected by NLTE, although departures in the line formation region are not large. Low-excitation levels of Co II are in thermal equilibrium with its ground state. But, most of the higher Co II levels are overpopulated due to non-equilibrium excitation processes. This NLTE mechanism is typical for *majority* ions, i.e. ions of the dominant ionization stage of an element.

The tests performed with a smaller model constructed with 246 Co I levels and closed by the Co II ground state indicate poor performance of such a *reduced* atomic model. This changes ionization and excitation equilibria in both ions, which is manifested in spurious overpopulation of the Co II ground state and stronger thermalization of Co I levels. Thus, reduction of the atomic model, as is usually done for 3D NLTE calculations, must be performed with extreme caution.

The uncertain parameters in our models are cross-sections for photoionization and collisions with neutral hydrogen atoms. Fig. 2b demonstrates the effect of stronger photoionization on the atomic level populations; here, cross-sections are multiplied by a scaling factor $S_p = 300$. The main difference with the reference model (Fig. 2a) is that depopulation of all levels is amplified at $-1 < \log \tau_{5000} < 0.4$. The influence of collisions with H I is fully understood from Fig. 2c. When the standard Drawins formula is used with the scaling factor $S_H = 1$, all levels at line formation depths $-2 > \log \tau_{5000} > 0$ are more strongly coupled to the continuum, but this scaling factor is too small for LTE to be reached completely.

4.1.2 Metal-poor stars

The character of processes leading to NLTE effects in Co does not change for stellar atmospheres with parameters of cool turnoff stars, which form the basis of our abundance analysis.

Fig. 2d demonstrates the effect of *increasing temperature* on the departure coefficients of selected Co I and Co II levels. At $T_{\text{eff}} = 6400$ K, the ionization equilibrium Co I/Co II is somewhat different from that of the solar model. Nearly 98% of Co atoms are in a singly ionized stage, hence the ground state of Co II is not sensitive to overionization from the Co I levels. The level a^3F_4 keeps its thermodynamic equilibrium value. However, departure coefficients in Co I show larger deviations from unity. The reason is that a stellar flux maximum is shifted to shorter wavelengths, thus overionization affects even the lowest metastable levels with $E_i \sim 1$ eV and $\lambda_{\text{thr}} \sim 1800$ Å. In contrast, in the solar model overionization is important only for the levels with $E_i \sim 3$ eV.

The influence of photoionization is more pronounced with *decreasing metallicity* (Fig. 2e). The dramatic depopulation of all levels occurs at the depths of line formation, $-1 < \log \tau_{5000} < 0$. The overionization from the lowest levels is balanced by increased net recombination to the higher levels that results in a small overpopulation of the latter at $\log \tau_{5000} \sim 0$. In the higher layers, $\log \tau_{5000} \sim -1$ even an overpopulation of the Co II ground state develops. Also, we note an increasing importance of line pumping in Co II. For example, the level $z^5D_4^o$ has $b_i \gg 1$ already at $\log \tau_{5000} \sim -0.3$. This is characteristic of all Co II levels with $E_i > 5$ eV. Hence, we expect *substantial NLTE effects in the lines of both Co I and Co II* in metal-poor stars.

A combination of low effective temperature, low gravity, and low metal content leads to a rather disorderly behavior of departure coefficients for different levels (Fig. 2f). Such stellar parameters are representative of giants where the collisional interaction is much weaker compared to dwarfs. Each level of Co I is no longer coupled to the bulk of levels with similar energies, but displays a distinct behaviour that is determined by the competition of radiative b-f and b-b processes. As a result, *NLTE line formation for giants*

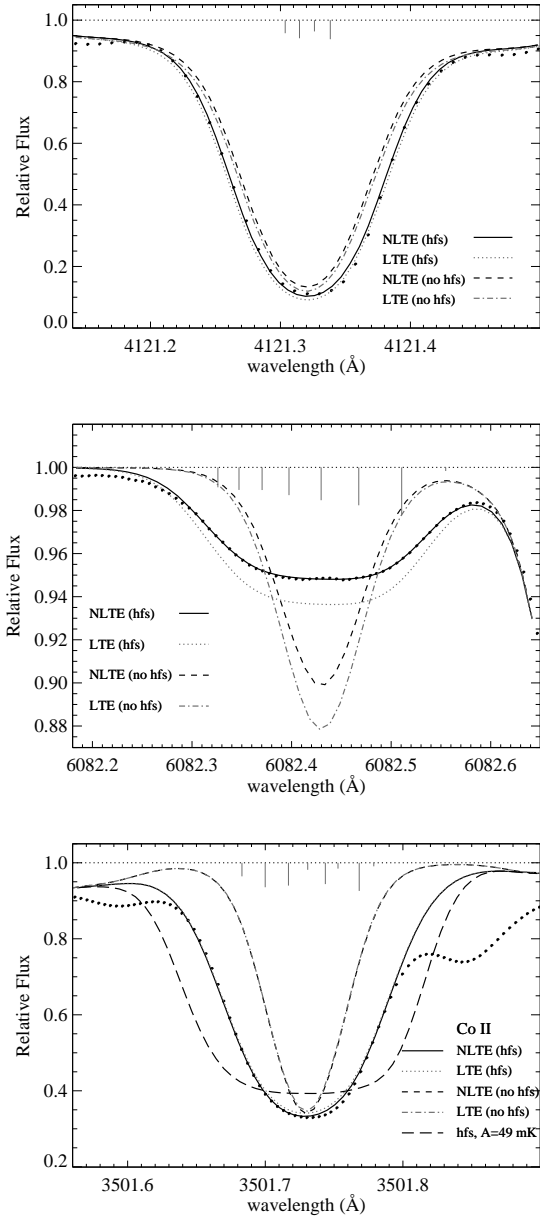


Figure 3. The lines of Co I (4121, 6082 Å) and Co II (3501 Å) in the solar flux spectrum (filled circles). Synthetic NLTE and LTE profiles with and without HFS are labeled correspondingly. Wavelength positions and relative line strengths of the HFS components are indicated. Note that the relative HFS component intensities are not on the same scale in figures. The long-dashed trace on the bottom figure indicates the NLTE profile computed with $A = 49$ mK for the lower level a^5P_3 (our reference value is $A = 40$ mK).

and dwarfs can be different for transitions involving different levels. This is evident by comparing the runs of b_i for the levels of e^6G , $z^2G_{9/2}$, and a^3F terms in Fig. 2e and 2f.

4.2 NLTE and HFS effects on the line formation

The computed profiles for selected lines of Co I and Co II are compared with the solar spectrum in Fig. 3. The synthetic profiles were calculated under LTE and NLTE conditions, with and without HFS.

Table 4. NLTE abundance corrections for lines of Co I and Co II calculated with selected models of the grid. Hyphens refer to the lines with computed NLTE equivalent widths below 1 mÅ. Collisions with neutral hydrogen are included with the reference scaling factor $S_H = 0.05$. Note that Δ_{NLTE} for the Co II line at 3501 Å are also given for the cases when its equivalent width is below 1 mÅ.

$T_{\text{eff}}/\log g/[\text{Fe}/\text{H}]$ wavelength, Å	Δ_{NLTE}					
	3501	3845	3957	4020	4110	4121
4800/1.8/-3.3	0.12	0.92	0.82	-	0.88	0.88
5000/3/0	-0.03	0.07	0.11	0.11	0.15	0.07
5000/3/-1	-0.03	0.20	0.26	0.25	0.28	0.22
5000/3/-2	0.02	0.64	0.60	0.64	0.48	0.76
5000/3/-3	0.13	1.03	0.85	-	0.69	0.85
5000/4/0	-0.04	0.03	0.05	0.08	0.15	0.04
5000/4/-1	-0.04	0.13	0.17	0.18	0.28	0.15
5000/4/-2	-0.03	0.45	0.44	0.47	0.48	0.62
5000/4/-3	0.08	0.67	-	-	0.69	0.66
5500/4/0	-0.03	0.08	0.12	0.12	0.23	0.1
5500/4/-1	-0.01	0.27	0.3	0.32	0.36	0.35
5500/4/-2	0.02	0.66	-	0.63	0.63	0.67
5500/4/-3	0.17	0.75	-	-	-	0.74
5780/4.4/0	-0.02	0.11	0.14	0.12	0.23	0.1
6000/4/0	-0.02	0.1	0.15	0.18	0.22	0.13
6000/4/-1	0.01	0.4	0.39	0.39	0.4	0.47
6000/4/-2	0.06	0.64	-	-	0.63	0.63
6000/4/-3	0.31	0.69	-	-	-	0.7
6200/3.4/0	-0.02	0.15	0.17	0.18	0.23	0.16
6200/3.4/-1.2	0.01	0.5	0.47	0.46	0.47	0.52
6200/3.4/-2.4	0.11	0.65	-	-	-	0.64
6200/4.6/0	-0.01	0.1	0.13	0.13	0.17	0.12
6200/4.6/-1.2	0.01	0.43	0.42	0.41	0.42	0.46
6200/4.6/-2.4	0.11	0.61	-	-	-	0.59
6400/4.2/0	-0.01	0.15	0.17	0.18	0.2	0.15

All lines selected for the abundance analysis in the Sun and metal-poor stars are relatively weak (Table 2). Hence, the Co I lines computed under NLTE behave similarly: they are uniformly weakened compared to the LTE profiles. The main effect is the shift of the optical depth scale due to $b_i < 1$ at line formation depths. As a result, the NLTE abundance corrections² Δ_{NLTE} are positive; for the majority of Co I lines computed with the solar model atmosphere, $\Delta_{\text{NLTE}} \sim +0.15$ dex.

NLTE abundance corrections for different stellar parameters are given in Table 4. These values are computed only for five Co I lines and one Co II line, which can be detected in our spectra of stars with $[\text{Fe}/\text{H}] < -0.5$. Although it is not our goal to investigate giant stars, we have performed test calculations for the *cool giant model* ($T_{\text{eff}} = 4800$ K, $\log g = 1.8$, $[\text{Fe}/\text{H}] = -3.3$). This exception is made because many analyses of Co abundances refer to bright cool giants with low $[\text{Fe}/\text{H}]$. NLTE corrections from Table 4 should only be used to get a crude estimate of deviations from LTE in metal-poor stars due to the dependence of NLTE correction on the Co abundance.

The main stellar parameter that determines the sign and magnitude of the NLTE abundance corrections is metallicity. Low metal abundances lead to decreasing number density of free electrons and

² The difference in abundances required to fit NLTE and LTE profiles is referred to as the NLTE (abundance) correction $\Delta_{\text{NLTE}} = \log e^{\text{NLTE}} - \log e^{\text{LTE}}$.

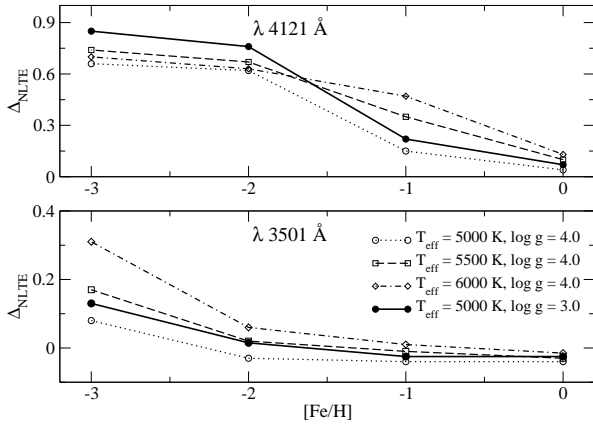


Figure 4. NLTE abundance corrections Δ_{NLTE} calculated for the lines of Co I (4121 Å, top) and Co II (3501 Å, bottom). Calculations are performed for sixteen models with $T_{\text{eff}} = 5000, 5500, 6000$ K, $\log g = 3, 4$, $[\text{Fe}/\text{H}] = 0, -1, -2, -3$.

reduced line absorption in the UV, so that the effect of overionization on the *opacity* of Co I lines monotonously increases. On average, Δ_{NLTE} increases with decreasing $[\text{Fe}/\text{H}]$ from ~ 0.1 dex for $[\text{Fe}/\text{H}] = 0$ to ~ 0.7 dex for $[\text{Fe}/\text{H}] = -3$ (Fig. 4 top). It is clear that in addition to the effect of metallicity, high temperatures control overionization at higher $[\text{Fe}/\text{H}]$, whereas at low $[\text{Fe}/\text{H}]$ the effect of low $\log g$ is more important.

The response of NLTE corrections for Co I to the effective temperature is not uniform. At moderate gravities ($\log g = 4$), the NLTE corrections are maximal in the warm model $T_{\text{eff}} = 5500$ with the smallest metallicity (see Table 4). Lower NLTE corrections at even higher temperatures are due to the increased rates of collisions. At low temperatures, NLTE abundance corrections are also smaller because the stellar flux maximum is shifted to longer wavelengths, away from ionization thresholds of the important Co I levels.

NLTE corrections increase with decreasing surface gravity. However, for different metallicities and *supersolar* temperatures, reduction of $\log g$ from 4.6 to 3.4 changes the NLTE abundance corrections for all lines only by $\sim 0.03 - 0.06$ dex. In contrast, Δ_{NLTE} strongly depends on stellar gravity in the *cool* model with $T_{\text{eff}} \leq 5000$. The extreme values of Δ_{NLTE} are found for the cool giant model with a subsolar temperature $T_{\text{eff}} = 4800$ K, $[\text{Fe}/\text{H}] = -3.3$, and a very low gravity $\log g = 1.8$. This is an expected result, because all collisional interactions become very weak due to the small metallicity and gravity, and the role of radiative processes increases in spite of the reduced temperature.

The NLTE corrections for the Co II line show a different behaviour, which is related to the deviation of line source function S^1 from the Planck function $B_\nu(T_e)$. As an example, we study the formation of the Co II line at 3501 Å. It *seems* to be relatively unblended in the solar spectrum and can be used to test the ionization equilibrium of Co in the metal-poor stars. In the solar model, this line is sufficiently strong; its core is formed in the upper layers $\log \tau_{5000} \sim -2$, where spontaneous transitions depopulate the upper level, thus $b_i > b_j$ and $S^1 < B_\nu(T_e)$. Therefore, line core intensities are slightly larger in NLTE (Fig. 3 bottom), and $\Delta_{\text{NLTE}} < 0$ (Fig. 4 bottom). At $[\text{Fe}/\text{H}] \leq -1$, NLTE abundance corrections start to increase smoothly. Due to less UV opacity, the radiation field

is amplified producing overpopulation of the higher levels via the photon pumping mechanism, $b_i < b_j$. The line source function becomes superthermal, $S^1 > B_\nu(T_e)$, and the line is weakened compared to the LTE case. The same mechanism is responsible for the positive NLTE abundance corrections in the models with $[\text{Fe}/\text{H}] \leq -2$. At very low metallicities (Fig. 4 bottom), NLTE corrections are as large as $+0.2 \dots +0.3$ dex, depending on the temperature. Consequently, *the analysis of Co II lines in very metal-poor stars can lead to substantial errors in abundances if NLTE effects are neglected.*

The errors in abundances introduced by neglecting HFS depend on the line strength. For the solar model, the abundances derived for saturated lines 4121 Å and 3501 Å without HFS are overestimated by 0.4 dex and 0.9 dex, respectively. The reason is that HFS effectively de-saturates strong lines leading to a compound profile, where the strength of each component is more linearly proportional to the element abundance. Note also that saturated lines are also sensitive to the A and B factors used in calculations of HFS. For example, the 3501 Å HFS line computed with an approximate estimate $A = 49$ mK for the lower level a^5P_3 (taken from Pickering et al. 1998) cannot fit the observed profile at all (Fig. 3 bottom). In contrast, our new reference value $A = 40$ mK provides an excellent fit to the observed profile. The weak lines, like 6082 Å, are less affected: the profile computed with all HFS components gives ~ 0.1 dex lower abundance. At low metallicity, $[\text{Fe}/\text{H}] = -2$, the abundances are almost insensitive to inclusion of HFS in spectrum synthesis; the errors for all investigated lines are not larger than 0.05 dex.

4.3 Solar abundance of Co

The solar spectrum is calculated using the MAFAGS-ODF model atmosphere with $T_{\text{eff}} = 5780$ K, $\log g = 4.44$, $[\text{Fe}/\text{H}] = 0$, and a constant microturbulence velocity $\xi_t = 0.9$ km s $^{-1}$ for all lines. The Co line profiles are broadened by a rotation velocity $V_{\text{rot}} = 1.8$ km s $^{-1}$, and by a macroturbulence velocity $V_{\text{mac}} = 2.5 \dots 4$ km s $^{-1}$. The observed flux spectrum is taken from the Kitt Peak Solar Flux Atlas (Kurucz et al. 1984).

The lines of Co I and Co II selected for abundance calculations are listed in Table 2. Measured oscillator strengths are available only for 17 out of 20 lines. Two reference sources of experimental $\log gf$ values are Cardon et al. (1982) and Nitz et al. (1999). For three yellow lines of multiplet 158 we had to adopt the theoretical values of Kurucz & Peytremann (1996). However, the accuracy of calculated data is unknown, hence the lines of multiplet 158 are only used in the differential abundance analysis of metal-poor stars. Our final estimate of the solar Co abundance is based solely on the experimental $\log gf$ values. Three lines in the near-UV, 3845, 3957, and 4066 Å, are also neglected in solar calculations due to severe blending.

Figure 5 shows NLTE and LTE abundances for 16 lines of Co I as a function of their oscillator strengths. A weak trend of individual abundances with gf values, as well as similar line-to-line scatter under NLTE and LTE, points at the errors in $\log gf$'s. For the weak lines, the errors are $\sim 15 - 25\%$ (Cardon et al. 1982). Two weak lines at 6189 and 6814 Å show NLTE and LTE abundances deviating from the mean by ≥ 0.1 dex. The lines at 7417 and 7712 Å contain a well-resolved blend in their wings, which is, however, not present in our linelist. The line at 5369 Å gives very large abundance, 5.15 dex. As its gf -value seems to be reliable, it is likely that the line contains an unidentified blend. We ignore these five lines in the solar analysis, and our sample is further reduced to 11 lines. No

significant correlation of individual NLTE or LTE abundances is found with the excitation potential of the lower level or equivalent width of the lines.

The average NLTE and LTE abundances of Co in the solar atmosphere are $\log \varepsilon_{\text{Co},\odot}^{\text{NLTE}} = 4.95 \pm 0.04$ dex and $\log \varepsilon_{\text{Co},\odot}^{\text{LTE}} = 4.81 \pm 0.05$ dex, respectively. The standard deviations are quoted as errors. When calculated only with the $\log gf$ data from Cardon et al. (1982), $\log \varepsilon_{\text{Co},\odot}^{\text{NLTE}} = 4.96 \pm 0.06$ dex. This value is nearly equal to the NLTE abundance calculated using 5 lines with oscillator strengths from Nitz et al. (1999), $\log \varepsilon_{\text{Co},\odot}^{\text{NLTE}} = 4.98 \pm 0.03$.

It is interesting that there is a large difference of 0.14 dex between the solar NLTE and LTE abundances determined from the Co I lines with $S_{\text{H}} = 0.05$. Up to now, such a strong NLTE abundance effect has been demonstrated only for Sc I, with $\Delta_{\text{NLTE}} \sim 0.18$ dex derived using $S_{\text{H}} = 0.1$ (Zhang et al. 2008). The average solar NLTE corrections for the other Fe-peak elements, Fe (Gehren et al. 2001) and Mn (Bergemann & Gehren 2007), are smaller. This is, however, not surprising because the magnitude of NLTE effects strongly depends on the *model atom used in calculations*, in particular, on the collision efficiency with hydrogen atoms S_{H} (see Sect. 3.2) and the detailed atomic properties, like separation of energy levels, number and strength of transitions, and ionization potential. Weaker NLTE effects for Mn I ($\Delta_{\text{NLTE}} \sim 0.05$ dex) compared to Co I are due to the differences in the atomic models: a) the number of low-excitation levels, which stipulate overionization; b) collisional coupling to the continuum (the latter issue was also emphasized in Gehren et al. 2001), which amplifies recombination; c) the general number of levels. The model of the Fe I atom used by Gehren et al. (2001) is different from our Co I model (at least) in the following aspects. The authors adopted $S_{\text{H}} = 5$ as their final value *and* forced thermalization of the Fe I levels with excitation energy above 7.3 eV. Assuming *no* explicit thermalization, as we do in the current work, Gehren et al. (2001) obtain *very strong NLTE effects* on Fe I lines even for the model with $S_{\text{H}} = 5$, $\Delta_{\text{NLTE}} \sim 0.12$ dex. Using this large scaling factor for H I collisions, we derive the average NLTE abundance correction for Co I lines $\Delta_{\text{NLTE}} \sim 0.06$ dex. Thus, we see no reason to force thermalization of the upper Co I levels. In contrast, we consider collisions with H I as the main source of $\log \varepsilon_{\text{Co},\odot}^{\text{NLTE}}$ uncertainty. We performed a series of NLTE abundance calculations with $0 \leq S_{\text{H}} \leq 5$. The NLTE result for $S_{\text{H}} = 0$, $\log \varepsilon_{\text{Co},\odot}^{\text{NLTE}} = 4.96 \pm 0.04$, is almost identical to the case of $S_{\text{H}} = 0.05$. Also, with increasing scaling factor from 0.5 to 5, the abundance steadily decreases from 4.91 to 4.87 dex with the standard deviation remaining constant, $\sigma \approx 0.04$ dex. Thus, no conclusion can be drawn concerning the optimum value of the scaling factor to hydrogen collisions.

The majority of Co I lines are weak, and they are not sensitive to the van der Waals damping, neither are they affected by the microturbulence. We found only one line at 4121 Å, which gives different abundances with the variation of ξ_{t} or $\log C_6$. For $\Delta \xi_{\text{t}} = \pm 0.2$ km s⁻¹, $\Delta \log \varepsilon = \mp 0.1$ dex; $\Delta \log C_6 = \pm 0.5$ corresponds to $\Delta \log \varepsilon = \mp 0.12$ dex. With $\log C_6 = -31.63$ calculated using Anstee & O'Mara (1995) theory and $\xi_{\text{t}} = 0.9$ km s⁻¹, this line gives a NLTE abundance of 4.95 dex, which is consistent with abundances derived from the other Co I lines. Moreover, the standard deviation of the *average* Co NLTE abundance, $\sigma = 0.04$ dex, is already smaller than the errors given for the oscillator strengths. Hence, we have not tried to adjust damping constants and microturbulence any further.

We checked the *ionization equilibrium* of Co for the Sun, using the relatively unblended line of ionized cobalt Co II at 3501 Å (Fig. 3 bottom). The line is saturated and consists of 8 HFS com-

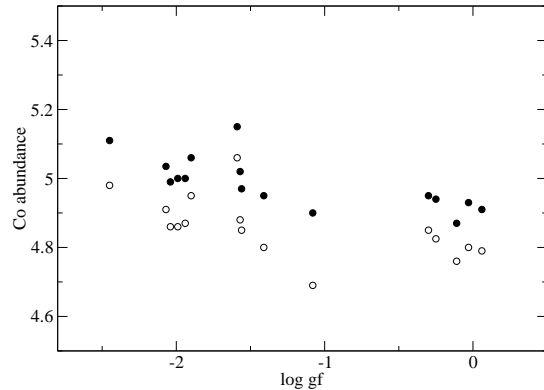


Figure 5. Abundances of the 17 solar Co I lines. NLTE and LTE abundances are marked with filled and open circles, respectively.

ponents, which were calculated with our new hyperfine splitting constants. To produce a better fit to the observed profile, the A factor for the upper level was decreased by 1 mK; this is within the errors of the measured HFS value. Using the theoretical oscillator strength from Raassen et al. (1998), $\log gf = -1.22$, we derive $\log \varepsilon_{\text{Co},\odot}^{\text{NLTE}} = 4.86$ and $\log \varepsilon_{\text{Co},\odot}^{\text{LTE}} = 4.88$ dex. With the experimental gf -value from Salih et al. (1985), $\log gf = -1.18$, the NLTE and LTE abundances are $\log \varepsilon_{\text{Co},\odot}^{\text{NLTE}} = 4.82$ and $\log \varepsilon_{\text{Co},\odot}^{\text{LTE}} = 4.84$ dex, respectively. We do not assign any error to these values for the reasons described in the following paragraph.

The ~ 0.1 dex discrepancy between the lines of Co I and Co II in NLTE is most likely due to the erroneous abundance from the Co II line. First, the uncertainty due to the continuum placement and blending in the near-UV window of the solar spectrum is large. At present, there is no information about other strong lines overlapping with the 3501 Å line of Co II. However, if atomic physics experiments or theoretical calculations reveal the presence of a strong blend, the Co abundance determined from the UV Co II line will be reduced. The accuracy of the calculated oscillator strength provided by Raassen et al. (1998) is not known, whereas the accuracy of the Salih et al. (1985) gf -value for the 3501 Å line is not better than 50%, which translates to abundance uncertainty of ~ 0.2 dex. If the problem is concealed in hydrogen collisions, a very large scaling factor $S_{\text{H}} \geq 5$ is needed to bring two ionization stages in agreement. This issue will be further investigated in the next section devoted to the metal-poor stars.

The abundance of Co in C I meteorites is 4.89 ± 0.01 dex (Lodders et al. 2009). It conforms to our NLTE abundance $\log \varepsilon_{\text{Co},\odot}^{\text{NLTE}} = 4.95 \pm 0.04$ dex derived from Co I lines within the combined errors of both values. Also, the LTE abundance from the Co II line (4.88 dex) agrees to meteoritic, if the theoretical gf -value from Raassen et al. (1998) is used. Previously, the photospheric LTE abundance from the Co I lines was determined by Cardon et al. (1982), $\log \varepsilon_{\text{Co},\odot} = 4.92 \pm 0.08$ dex. This value is ~ 0.1 dex higher than our LTE abundance, which is due to several reasons. First, the authors used the semi-empirical model atmosphere of Holweger (1967), which is the essentially the same as the model of Holweger & Müller (1974). The latter model is known to give higher abundances compared to the theoretical model atmospheres. Second, equivalent widths were used to measure the abundances. This method always gives only an *upper* limit on the abundance,

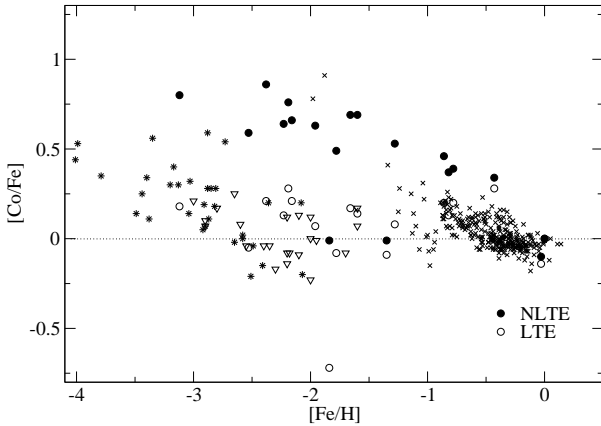


Figure 6. $[\text{Co}/\text{Fe}]$ vs. $[\text{Fe}/\text{H}]$ in metal-poor stars. The Co abundances are derived from Co I lines under NLTE (filled circles) and LTE (open circles). Iron abundances are determined from Fe II lines in LTE. The sources of other LTE $[\text{Co}/\text{Fe}]$ data are: Johnson 2002 (open triangles), Reddy et al. 2003, 2006 (crosses), McWilliam et al. 1995 (stars).

because the contribution to a line strength from blending lines is neglected. In all other respects (oscillator strengths, microturbulence, line set), our study and the analysis of Cardon et al. (1982) are similar.

4.4 Abundances in metal-poor stars

Our sample of 17 objects from Bergemann (2008) was expanded by one subdwarf G 64-12 with $[\text{Fe}/\text{H}] = -3.12$. The UVES spectrum for G 64-12 was taken from ESO/ST-ECF Science Archive Facility (PID 67.D-0554(A)). Other stars were observed with the UVES echelle spectrograph (ESO VLT UT2, Chile) in 2001, and/or with the FOCES echelle spectrograph (CAHA observatory, Calar Alto) during 1999 and 2000. The data for HD 61421 and HD 84937 were taken from the UVESPOP survey (Bagnulo et al. 2003). The UVES data cover a spectral range from 3300 to 6700 Å, whereas FOCES spectra are cut at 4000 Å. A detailed description of the observational material can be found in Bergemann (2008) and Bergemann & Gehren (2008).

The abundance ratios for Co with respect to Fe in stars of our sample are given in Table 3. The Co abundances of thick disk stars with $-1 < [\text{Fe}/\text{H}] < -0$ are based on 6 to 10 lines, which have $W_\lambda > 20$ mÅ in the solar spectrum. In the spectra of the halo stars, only a few lines of Co I ($\lambda\lambda$ 3845, 4020, 4110, 4121) are detected. Due to a systematic abundance offset of ~ 0.2 dex between the line at 4110 Å and other Co I lines, this near-UV line was excluded from stellar analysis. The discrepancy might be related to the poor modelling of H_δ inner wings, where the 4110 Å line is located, or to a blend. In fact, no Co abundance studies in metal-poor stars include the line at 4110 Å. For G 64-12, the abundance is based on the single Co I line at 3845 Å, and the error bar ± 0.1 dex reflects the uncertainty of the line fitting due to the low S/N ($S/N \sim 120$) in the near-UV spectral window. We could not determine the solar $\log(gf\varepsilon)_\odot$ value for the 3845 Å line, hence all stellar abundances based on the line were calculated using the experimental $\log gf = 0.01$ from Cardon et al. (1982).

The $[\text{Co}/\text{Fe}] - [\text{Fe}/\text{H}]$ relation, along with the results of other authors, is demonstrated in Fig. 6. Note that the solar NLTE and

LTE $[\text{Co}/\text{Fe}]$ values are set to 0 by definition. The NLTE abundances of Co in the metal-poor stars are higher than the LTE abundances by 0.4 – 0.7 dex. Thus, instead of the flat $[\text{Co}/\text{Fe}]$ trend in metal-poor stars, we find that the $[\text{Co}/\text{Fe}]$ ratio increases with decreasing metallicity down to $[\text{Fe}/\text{H}] \sim -2$ and is roughly constant thereafter. Two stars with very low NLTE and LTE $[\text{Co}/\text{Fe}]$ ratios are HD 25329 and HD 103095. These stars were also analysed by Peterson (1981), who derived $[\text{Co}/\text{Fe}] = +0.48$ and $[\text{Co}/\text{Fe}] = +0.15$ for HD 25329 and HD 103095, respectively. The discrepancy with our values stems from different model parameters and abundance analysis techniques. In particular, Peterson used $\log gf$ values calibrated on solar lines to calculate the abundances from line equivalent widths, and Unsöld approximation for $\log C_6$ values was assumed.

Our LTE abundances are generally consistent with LTE results of the other authors considered here, although in the metal-poor domain Co abundances show a large scatter within a study and between studies (Fig. 6). The general trend is hard to define, although the majority of studies indicate that Co is increasing with respect to iron towards very low metallicities. For the thick disk stars our $[\text{Co}/\text{Fe}]$ trend with $[\text{Fe}/\text{H}]$ is flat and slightly supersolar, in agreement with Reddy et al. (2006). The thin disk star, Procyon, supports mild underabundance of Co in the thin disk as follows from the results of Reddy et al. (2003). The average Co abundances for stars $[\text{Fe}/\text{H}] < -1$ are consistent with Johnson (2002) as to slope, absolute values, and dispersion. Note that Johnson analyzed only giants.

In the attempt to check the ionization equilibrium of Co, we calculated differential abundances from the 3501 Å line of Co II. This line can still be discerned from the continuum only in the spectra of 5 stars. Thus, these abundances must be treated, at best, as upper limits because of poor S/N below 4000 Å. The NLTE abundance corrections for Co II are not so small and positive. For HD 84937 and HD 140283, $\Delta[\text{Co}/\text{Fe}]_{\text{II}}(\text{NLTE} - \text{LTE})^3 = +0.14$ and $+0.11$ dex, respectively. Whereas, for HD 102200, HD 34328, and HD 122563, the NLTE corrections are $+0.04 \dots +0.07$ dex. A significant discrepancy still remains between abundances determined from the lines of Co I and Co II.

Consistent ionization equilibria under NLTE require either significantly lower abundances from the neutral lines and/or much higher abundances from the ionic line. The former can be achieved with increasing the scaling factor to the H I collision cross-sections, S_{H} . Test calculations were performed for two stars. The NLTE results for HD 34328 computed with $S_{\text{H}} = 1$ are not very different from the case of $S_{\text{H}} = 0.05$ (our reference value): the abundance from the Co I lines decreased by 0.15 dex. It is only with $S_{\text{H}} = 10$ that the discrepancy is solved: $[\text{Co}/\text{Fe}]_{\text{I}}^{\text{NLTE}} = 0.26$, which is in agreement with $[\text{Co}/\text{Fe}]_{\text{II}}^{\text{NLTE}} = 0.21$. The abundances derived from Co II lines are not sensitive to a variation of S_{H} . However, for HD 84937, assumption of $S_{\text{H}} = 10$ leads to $[\text{Co}/\text{Fe}]_{\text{I}} = 0.27$, which is still ≈ 0.2 dex higher than the NLTE abundance determined from Co II lines. Whether such a large scaling factor is justified is questionable.

Another option is that our model atmospheres are not satisfactory, and granular inhomogeneities will have a large effect on abundances in addition to NLTE. Let us consider Fe, for which calculations of 1.5D NLTE line formation with 3D convective model atmospheres have been performed for the Sun and the metal-poor subgiant HD 140283. Using the Fe I lines Shchukina et al. (2005)

³ Co abundance ratios determined from the Co I and Co II lines are denoted as $[\text{Co}/\text{Fe}]_{\text{I}}$ and $[\text{Co}/\text{Fe}]_{\text{II}}$, respectively

found equal 3D and 1D NLTE abundances for both stars that were interpreted as due to *stronger* NLTE effects in 3D than in 1D models, which exactly cancel large 3D corrections. However, large positive NLTE abundance corrections of $\sim +0.4$ dex were demonstrated at low metallicity for weak Fe II lines in 3D. Recalling that Co I and Fe I have a very similar complex atomic structure with ionization energies differing by ~ 0.04 eV, one may expect that 3D will have the same (minor) effect on NLTE-based abundances of Co determined from Co I lines. Whereas, *large positive 3D corrections may be necessary for Co II lines*. In this case, our metallicities based on LTE abundances from Fe II lines may not necessarily be wrong, because the magnitude of the NLTE effect depends strongly on the choice of the scaling factor S_H to the hydrogen collision cross-sections. This parameter must be separately calibrated on the solar and stellar spectra, and for Fe it may take the values different from that used for Co.

We have also investigated the effect of a temperature enhancement on the abundance analysis by repeating the calculations for HD 102200 with $\Delta T_{\text{eff}} = \pm 100$ K with respect to our reference value $T_{\text{eff}} = 6120$ K. For both ions the effect turned out to be negligible. With $T_{\text{eff}} = 6220$ K, abundances for Co I lines increased respectively by 0.02 and 0.06 dex, and the abundances from the Co II line decreased by ~ 0.02 dex. Abundance corrections of the same magnitude but with the reverse sign were derived for lower T_{eff} . Thus, we cannot attribute the ionization equilibrium problem to systematic errors in T_{eff} .

5 COMPARISON WITH CHEMICAL EVOLUTION MODELS

There are several models in the literature that describe the evolution of Co in the Galaxy. The difference between theoretical trends is strikingly large: both the shape of the [Co/Fe] trend and the magnitude of Co depletion or overproduction relative to Fe in metal-poor stars vary by an order of magnitude. In fact, *neither of the GCE models are able to describe our NLTE [Co/Fe] trend in metal-poor stars*. The Goswami & Prantzos (2000) model with metallicity-independent SNE yields gives only a qualitatively similar behaviour, characterized by increase of [Co/Fe] ratios towards low metallicities. However, this model gives a very good fit to the LTE Co abundances from the current work and other sources. Closer to our NLTE results is the model of François et al. (2004) with unadjusted metallicity-independent SN yields, but the offset between theoretical calculations and the spectroscopic abundances is still too large, ~ 0.25 dex. The chemical evolution models with metallicity-dependent SN yields (Timmes et al. 1995; Samland 1998; Goswami & Prantzos 2000) predict radically different [Co/Fe] trends, which are ruled out both by NLTE and LTE spectroscopic abundances of Co. The same is true for the results of Arnett (1971) Co evolution calculations, whether with or without hydrostatic carbon burning. This discrepancy was also noted by Arnett et al. (1971) and Arnett (1971), who proposed that the [Co/Fe] ratio should be strongly correlated with the SN Ia progenitor metal content and the amount of mixing in the ISM. However, the effect that this would have on the abundances in metal-poor stars is unclear.

The conclusion from the NLTE trend of Co in metal-poor stars is that massive stars overproduce Co relative to Fe. The observed decline of [Co/Fe] at [Fe/H] ~ -1 can be explained by an underproduction of Co in SN Ia, but the possibility that SN II and SN Ia Co yields are metallicity-dependent is also not excluded. However, we

see that all chemical evolution models, which utilize metallicity-dependent yields, are inadequate to describe the [Co/Fe] trend suggesting that *the problem is in the stellar yields*. This is not unexpected, given the sensitivity of supernova yields to the details of explosion. Woosley & Weaver (1995) emphasized that their SN II iron yields could be in error by a factor of 2, ascribing even larger uncertainties to the elements produced in α -rich freeze-out due to the great sensitivity of those to the mass cut placement. For deeper mass cuts, more Co is produced. Nakamura et al. (1999) found that an increasing neutron excess increases the Co production. Umeda & Nomoto (2003, 2005) showed that if a large-scale uniform mixing occurs in the inner layers of very massive stars, $M > 25M_{\odot}$, then Co is produced more efficiently and the effect is even enhanced for larger explosion energies. In connection with this, Nagataki et al. (1997) demonstrated that the axisymmetric explosion in SN II models also boosts an α -rich freeze-out, and hence an increased production of Co. Interestingly, the results of massive star nucleosynthesis calculations performed by Heger & Woosley (2008) suggest that there is no need for hypernova to explain element abundance patterns in extremely metal-poor stars. The variety of mechanisms, which could affect the Fe-peak production, is overwhelming (Thielemann et al. 2007). Thus it is not hard to believe that the disagreement between observations and predictions of chemical evolution models is, at least in part, due to the deficiencies of the latter.

6 CONCLUSIONS

Deviations from LTE for Co I are controlled by overionization in the whole range of stellar parameters considered in this work. Thus, ionization equilibrium of Co is shifted towards lower number densities of Co I atoms compared to LTE. Excitation equilibrium of Co II is also disturbed due to optical line pumping.

NLTE effects on the line formation occur for lines of both ionization stages. For Co I, reduced line opacity stipulated by the overionization leads to general weakening of lines. Lines of Co II are affected by the deviation of line source functions from the Planck function. In the solar model atmosphere, these deviations are small, and it is safe to adopt LTE for Co II. In the models with very low metallicities and supersolar temperatures, NLTE corrections for Co II lines are as large as +0.3 dex. NLTE abundance corrections for the lines of Co I vary from +0.1 to +0.6 dex depending on the metallicity and the effective temperature. Our results for the giant models with low T_{eff} , low $\log g$, and low [Fe/H] suggest that in atmospheres of giants deviations from LTE are *larger* than in dwarfs, although the main stellar parameter that controls the magnitude of NLTE effects in Co is metallicity.

The solar abundance of Co derived from the NLTE analysis of Co I lines is 4.95 ± 0.04 dex, which is 0.13 dex higher than the LTE abundance. The abundance calculated from the single relatively unblended Co II line in the solar spectrum is 4.86 dex. The discrepancy of 0.09 dex between lines of two ionization stages points either at a failure of the NLTE approach to describe the ionization equilibrium of Co, or to an erroneous theoretical oscillator strength for the Co II transition. The NLTE abundances calculated with different scaling factors to cross-sections for H I collisions, $0.05 \leq S_H \leq 5$, are in agreement with the Co abundance measured in C I meteorites, 4.89 ± 0.01 dex.

For the *solar-metallicity* stars, the incorrect treatment of hyperfine structure leads to large errors in abundances. For the lines with saturated cores, the neglect of HFS leads to an abundance

overestimate by > 0.5 dex. Even the weak lines in the solar spectrum are not free from HFS effects, showing differences of $0.05 \dots 0.15$ dex. The influence of HFS on the line profiles and abundances is negligible in the metal-poor stars; not exceeding 0.05 dex.

The differential abundance analysis of 17 stars with $-2.5 \leq [\text{Fe}/\text{H}] \leq 0$ demonstrated that the evolution of Co abundances in the Galaxy is radically different from all previously reported trends. The NLTE abundance ratios $[\text{Co}/\text{Fe}]$ are supersolar for the thick disk stars, and at low metallicities $[\text{Co}/\text{Fe}]$ are as large as 0.8 dex. This result suggests that Co is overproduced relative to Fe in short-lived massive stars. The GCE models, which utilize metallicity-dependent yields for SNe, predict a qualitatively different $[\text{Co}/\text{Fe}]$ trend for the metal-poor stars, characterized by a plateau or $[\text{Co}/\text{Fe}]$ depletion. We relate the discrepancy to the deficiency in SN yields.

ACKNOWLEDGMENTS

We appreciate the assistance of Dr. Paul Barklem in calculations of $\log C_6$ values for the investigated lines. This work is based on observations made with the European Southern Observatory telescopes obtained from the ESO/ST-ECF Science Archive Facility. JCP thanks Ben Earner and Heather Cheeseman who contributed to this study through their Master's project. JCP thanks STFC (PPARC of the UK) and The Leverhulme Trust for financial support for this work. We thank the referee for useful comments and corrections.

REFERENCES

- Abia C., Mashonkina L., 2004, MNRAS, 350, 1127
 Allen C. W., 1973, *Astrophysical quantities*. London: University of London, Athlone Press, 1973, 3rd ed.
 Alonso A., Arribas S., Martinez-Roger C., 1995, A&A, 297, 197
 Anstee S. D., O'Mara B. J., 1995, MNRAS, 276, 859
 Arnett W. D., 1971, ApJ, 166, 153
 Arnett W. D., Truran J. W., Woosley S. E., 1971, ApJ, 165, 87
 Asplund M., 2005, ARAA, 43, 481
 Bagnulo S., Jehin E., Ledoux C., Cabanac R., Melo C., Gilmozzi R., The ESO Paranal Science Operations Team 2003, *The Messenger*, 114, 10
 Bergemann M., 2008, *Physica Scripta Volume T*, 133, 014013
 Bergemann M., Gehren T., 2007, A&A, 473, 291
 Bergemann M., Gehren T., 2008, A&A, 492, 823
 Blackwell-Whitehead R. J., Toner A., Hibbert A., Webb J., Ivarsson S., 2005, MNRAS, 364, 705
 Böhm-Vitense E., 1958, *Zeitschrift für Astrophysik*, 46, 108
 Burbidge E. M., Burbidge G. R., Fowler W. A., Hoyle F., 1957, *Reviews of Modern Physics*, 29, 547
 Butler K., Giddings J., 1985, *Newsletter on Analysis of Astronomical Spectra*, University of London, 9
 Cardon B. L., Smith P. L., Scalo J. M., Testerman L., 1982, ApJ, 260, 395
 Cayrel R., Depagne E., Spite M., Hill V., Spite F., François P., Plez B., Beers T., Primas F., Andersen J., Barbuy B., Bonifacio P., Molaro P., Nordström B., 2004, A&A, 416, 1117
 Del Peloso E. F., Cunha K., da Silva L., Porto de Mello G. F., 2005, A&A, 441, 1149
 Drawin H. W., 1969, *Zeitschrift für Physik*, 225, 483
 ESA 1997, *VizieR Online Data Catalog*, 1239, 0
 François P., Matteucci F., Cayrel R., Spite M., Spite F., Chiappini C., 2004, A&A, 421, 613
 Fuhrmann K., 2004, *Astronomische Nachrichten*, 325, 3
 Gehren T., Butler K., Mashonkina L., Reetz J., Shi J., 2001, A&A, 366, 981
 Gehren T., Korn A. J., Shi J., 2001, A&A, 380, 645
 Gehren T., Liang Y. C., Shi J. R., Zhang H. W. and Zhao G., 2004, A&A, 413, 1045
 Gehren T., Shi J. R., Zhang H. W., Zhao G., Korn A. J., 2006, A&A, 451, 1065
 Goswami A., Prantzos N., 2000, A&A, 359, 191
 Gratton R. G., Carretta E., Eriksson K., Gustafsson B., 1999, A&A, 350, 955
 Gratton R. G., Sneden C., 1991, A&A, 241, 501
 Grupp F., 2004, A&A, 420, 289
 Heger A., Woosley S. E., 2008, ArXiv e-prints
 Holweger H., 1967, *Zeitschrift für Astrophysik*, 65, 365
 Holweger H., Müller E. A., 1974, *Sol. Phys.*, 39, 19
 Holweger H., Oertel K. B., 1971, A&A, 10, 434
 Iwamoto K., Brachwitz F., Nomoto K., Kishimoto N., Umeda H., Hix W. R., Thielemann F.-K., 1999, ApJS, 125, 439
 Johnson J. A., 2002, ApJS, 139, 219
 Kopfermann H., 1958, *Nuclear Moments*. New York: Academic Press
 Korn A. J., Shi J., Gehren T., 2003, A&A, 407, 691
 Kuhn H. G., 1962, *Atomic Spectra*. London: Kuhn, Longmans
 Kurucz R., Bell B., 1995, *Atomic Line Data* (R.L. Kurucz and B. Bell) Kurucz CD-ROM No. 23. Cambridge, Mass.: Smithsonian Astrophysical Observatory, 1995., 23
 Kurucz R. L., 1992, *Revista Mexicana de Astronomia y Astrofisica*, vol. 23, p. 45
 Kurucz R. L., Furenlid I., Brault J., Testerman L., 1984, *Solar flux atlas from 296 to 1300 nm*. National Solar Observatory Atlas, Sunspot, New Mexico: National Solar Observatory, 1984
 Kurucz R. L., Peytremann E., 1996, *VizieR Online Data Catalog*, 6010, 0
 Lai D. K., Bolte M., Johnson J. A., Lucatello S., Heger A., Woosley S. E., 2008, ApJ, 681, 1524
 Lodders K., Palme H., Gail H., 2009, ArXiv e-prints
 Mashonkina L., Zhao G., Gehren T., Aoki W., Bergemann M., Noguchi K., Shi J. R., Takada-Hidai M., Zhang H. W., 2008, A&A, 478, 529
 Mashonkina L. J., 1996, in Adelman S. J., Kupka F., Weiss W. W., eds, *M.A.S.S., Model Atmospheres and Spectrum Synthesis Vol. 108 of Astronomical Society of the Pacific Conference Series, Accurate Collisional Cross Sections: Important Input Data in NonLTE Calculations*. p. 140
 McWilliam A., Preston G. W., Sneden C., Searle L., 1995, AJ, 109, 2757
 Menzel D. H., Pekeris C. L., 1935, MNRAS, 96, 77
 Nagataki S., Hashimoto M.-A., Sato K., Yamada S., 1997, ApJ, 486, 1026
 Nakamura T., Umeda H., Nomoto K., Thielemann F.-K., Burrows A., 1999, ApJ, 517, 193
 Nave G., Sansonetti C. J., Griesmann U., 1997, *Fourier Transform Spectroscopy: Methods and Applications*, Opt. Soc. Am. Tech. Digest Ser., 3
 Nitz D. E., Kunau A. E., Wilson K. L., Lentz L. R., 1999, ApJS, 122, 557
 Nomoto K., Thielemann F.-K., Yokoi K., 1984, ApJ, 286, 644
 Peterson R. C., 1981, ApJ, 244, 989
 Pickering J. C., 1996, ApJS, 107, 811

- Pickering J. C., 1998a, *Phys. Scr.*, 57, 385
Pickering J. C., 1998b, *Phys. Scr.*, 58, 457
Pickering J. C., Raassen A. J. J., Uylings P. H. M., Johansson S., 1998, *ApJS*, 117, 261
Pickering J. C., Thorne A. P., 1996, *ApJS*, 107, 761
Prochaska J. X., McWilliam A., 2000, *ApJL*, 537, L57
Raassen A. J. J., Pickering J. C., Uylings P. H. M., 1998, *A&AS*, 130, 541
Reddy B. E., Lambert D. L., Allende Prieto C., 2006, *MNRAS*, 367, 1329
Reddy B. E., Tomkin J., Lambert D. L., Allende Prieto C., 2003, *MNRAS*, 340, 304
Rutten R. J., 2003, in Hubeny I., Mihalas D., Werner K., eds, *Stellar Atmosphere Modeling Vol. 288 of Astronomical Society of the Pacific Conference Series, Utrecht Radiative Transfer Courses*. p. 99
Ryan S. G., Norris J. E., Bessell M. S., 1991, *AJ*, 102, 303
Salih S., Lawler J. E., Whaling W., 1985, *Phys. Rev. A*, 31, 744
Samland M., 1998, *ApJ*, 496, 155
Schönrich R., Binney J., 2009, *MNRAS*, pp 203–222
Seaton M. J., 1962, in Bates D. R., ed., *Atomic and Molecular Processes The Theory of Excitation and Ionization by Electron Impact*. p. 375
Shchukina N. G., Trujillo Bueno J., Asplund M., 2005, *ApJ*, 618, 939
Shi J. R., Gehren T., Butler K., Mashonkina L. I., Zhao G., 2008, *A&A*, 486, 303
Steenbock W., Holweger H., 1984, *A&A*, 130, 319
Sundqvist J. O., Ryde N., Harper G. M., Kruger A., Richter M. J., 2008, *A&A*, 486, 985
Thielemann F.-K., Fröhlich C., Hirschi R., et al. 2007, *Progress in Particle and Nuclear Physics*, 59, 74
Timmes F. X., Woosley S. E., Weaver T. A., 1995, *ApJS*, 98, 617
Umeda H., Nomoto K., 2003, *Nature*, 422, 871
Umeda H., Nomoto K., 2005, *ApJ*, 619, 427
Unsöld A., 1955, *Physik der Sternatmosphären, mit besonderer Berücksichtigung der Sonne.* Berlin, Springer, 1955. 2. Aufl.
van Regemorter H., 1962, *ApJ*, 136, 906
VandenBerg D. A., Swenson F. J., Rogers F. J., Iglesias C. A., Alexander D. R., 2000, *ApJ*, 532, 430
Wang B., Silk J., 1993, *ApJ*, 406, 580
White H. E., Eliason A. Y., 1933, *Physical Review*, 44, 753
Woosley S. E., Weaver T. A., 1995, *ApJS*, 101, 181
Zhang H. W., Gehren T., Zhao G., 2008, *A&A*, 481, 489

This paper has been typeset from a \TeX / \LaTeX file prepared by the author.

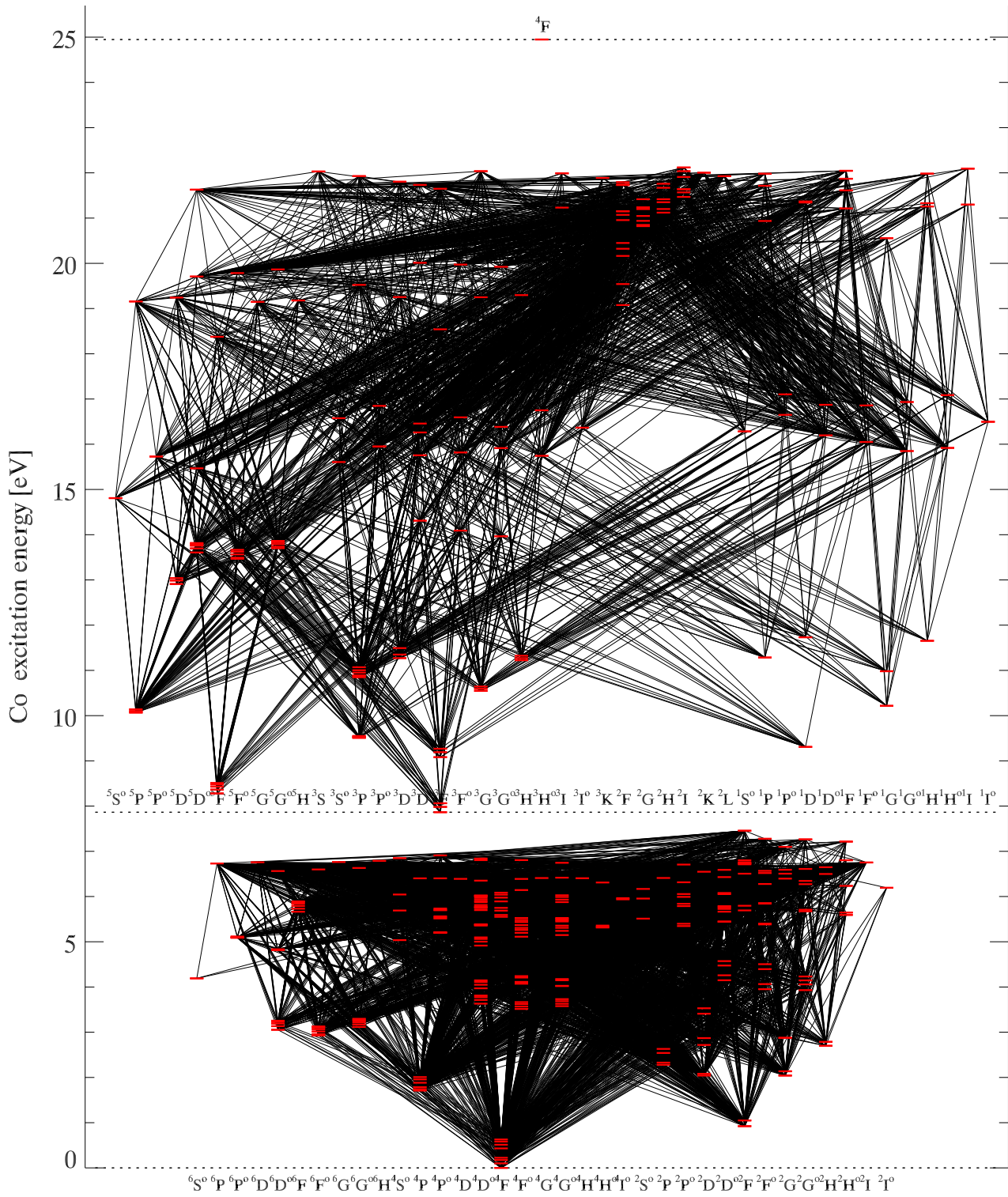


Figure A1. Grotrian diagram of the Co I/Co II model atom. Solid lines represent allowed and forbidden transitions included in the model atom. Ionization energies of Co I and Co II are 7.86 eV and 17.1 eV, respectively.

Table A1. HFS constants A and B (in units of 10^{-3} cm^{-1}) representing magnetic dipole and electric quadrupole interactions for Co I and Co II levels. Level energies E are given in eV. The interaction constants for all Co I levels are taken from Pickering (1996). For the Co II levels, the data measured in this work are used.

No.	level	g	E	A	B	No.	level	g	E	A	B
1	$a^4F_{9/2}$	10	0.00	15.	4.6	51	$z^4F_{3/2}^0$	4	3.67	14.2	0.0
2	$a^4F_{7/2}$	8	0.10	16.4	3.2	52	$z^4G_{11/2}^0$	12	3.58	25.8	7.
3	$a^4F_{5/2}$	6	0.17	20.5	2.3	53	$z^4G_{9/2}^0$	10	3.63	17.3	6.
4	$a^4F_{3/2}$	4	0.22	34.8	2.3	54	$z^4G_{7/2}^0$	8	3.69	15.	5.
5	$b^4F_{9/2}$	10	0.43	27.7	-4.	55	$z^4G_{5/2}^0$	6	3.73	13.3	5.
6	$b^4F_{7/2}$	8	0.51	22.3	-2.6	56	$z^4D_{7/2}^0$	8	3.63	25.1	0.
7	$b^4F_{5/2}$	6	0.58	18.8	-1.8	57	$z^4D_{5/2}^0$	6	3.71	23.2	1.
8	$b^4F_{3/2}$	4	0.63	10.2	-2.	58	$z^4D_{3/2}^0$	4	3.78	23.5	1.
9	$a^2F_{7/2}$	8	0.92	13.	-5.	59	$z^4D_{1/2}^0$	2	3.81	27.5	0.
10	$a^2F_{5/2}$	6	1.05	37.1	-3.	60	$z^2G_{3/2}^0$	10	3.93	16.5	0.
11	$a^4P_{5/2}$	6	1.71	5.9	-8.	61	$z^2G_{1/2}^0$	8	4.06	30.7	5.
12	$a^4P_{3/2}$	4	1.74	10.6	4.	62	$z^2F_{7/2}^0$	8	3.95	15.	6.
13	$a^4P_{1/2}$	2	1.79	-23.6	0.0	63	$z^2F_{5/2}^0$	6	4.06	34.9	0.
14	$b^4P_{5/2}$	6	1.88	37.4	5.	64	$y^4D_{7/2}^0$	8	3.97	16.	5.
15	$b^4P_{3/2}$	4	1.96	15.4	-2.	65	$y^4D_{5/2}^0$	6	4.05	15.5	0.
16	$b^4P_{1/2}$	2	2.01	57.6	0.0	66	$y^4D_{3/2}^0$	4	4.11	19.7	0.
17	$a^2G_{9/2}$	10	2.04	20.5	2.	67	$y^4D_{1/2}^0$	2	4.15	58.9	0.
18	$a^2G_{7/2}$	8	2.14	28.	-3.2	68	$y^4F_{9/2}^0$	10	4.07	9.9	8.
19	$a^2D_{3/2}$	4	2.04	13.	0.0	69	$y^4F_{7/2}^0$	8	4.11	17.	0.
20	$a^2D_{1/2}$	6	2.08	46.3	4.	70	$y^4F_{5/2}^0$	6	4.21	20.1	0.
21	$a^2P_{3/2}$	4	2.28	11.2	4.	71	$y^4F_{3/2}^0$	4	4.24	39.7	-2.
22	$a^2P_{1/2}$	2	2.33	20.1	0.0	72	$y^2G_{9/2}^0$	10	4.15	14.7	0.
23	$b^2P_{3/2}$	4	2.54	5.5	2.	73	$z^2D_{5/2}^0$	6	4.15	15.4	0.
24	$b^2P_{1/2}$	2	2.63	17.2	0.0	74	$z^2D_{3/2}^0$	4	4.26	46.1	2.
25	$a^2H_{11/2}$	12	2.70	22.6	0.0	75	$y^2D_{5/2}^0$	6	4.48	16.4	0.
26	$a^2H_{9/2}$	10	2.79	26.4	0.0	76	$y^2D_{3/2}^0$	4	4.57	42.	0.
27	$b^2D_{5/2}$	6	2.72	18.5	15.	77	$y^2F_{7/2}^0$	8	4.40	13.9	0.
28	$b^2D_{3/2}$	4	2.87	30.8	4.	78	$y^2F_{5/2}^0$	6	4.50	30.4	0.
29	$b^2G_{9/2}$	10	2.87	36.9	0.0	79	$x^4D_{7/2}^0$	8	4.92	10.1	0.
30	$b^2G_{7/2}$	8	2.88	8.8	0.0	80	$x^4D_{5/2}^0$	6	5.00	11.9	1.
31	$z^6F_{11/2}^0$	12	2.93	28.5	-2.	81	$x^4D_{3/2}^0$	4	5.06	17.6	0.
32	$z^6F_{9/2}^0$	10	2.96	28.5	4.	82	$x^4D_{1/2}^0$	2	5.1	55.8	0.
33	$z^6F_{7/2}^0$	8	3.02	26.4	5.	83	$e^4F_{9/2}^0$	10	5.55	13.4	0.
34	$z^6F_{5/2}^0$	6	3.07	24.	2.	84	$e^4F_{7/2}^0$	8	5.59	11.1	1.
35	$z^6F_{3/2}^0$	4	3.11	20.1	0.0	85	$e^4F_{5/2}^0$	6	5.69	18.4	0.
36	$z^6F_{1/2}^0$	2	3.13	-2.1	0.0	86	$e^4F_{3/2}^0$	4	5.75	35.5	0.
37	$z^6D_{9/2}^0$	10	3.05	28.1	0.0	87	$e^6F_{11/2}^0$	12	5.66	33.5	5.
38	$z^6D_{7/2}^0$	8	3.13	27.2	-3.	88	$e^6F_{9/2}^0$	10	5.73	31.5	2.
39	$z^6D_{5/2}^0$	6	3.19	26.6	-6.	89	$e^6F_{7/2}^0$	8	5.79	28.7	-1.
40	$z^6D_{3/2}^0$	4	3.23	27.	0.0	90	$e^6F_{5/2}^0$	6	5.84	25.7	-1.
41	$z^6D_{1/2}^0$	2	3.26	33.4	0.0	91	$e^6F_{3/2}^0$	4	5.87	19.4	-1.
42	$z^6G_{13/2}^0$	14	3.12	25.3	8.	92	$e^6F_{1/2}^0$	2	5.89	-17.1	0.
43	$z^6G_{11/2}^0$	12	3.17	23.	7.	93	$f^4F_{9/2}^0$	10	5.89	36.	5.
44	$z^6G_{9/2}^0$	10	3.22	20.6	5.	94	$f^4F_{7/2}^0$	8	5.98	28.3	3.
45	$z^6G_{7/2}^0$	8	3.25	18.3	6.	95	$f^4F_{5/2}^0$	6	6.04	19.5	3.
46	$z^6G_{5/2}^0$	6	3.28	14.4	3.	96	$f^4F_{3/2}^0$	4	6.09	-1.5	0.
47	$z^6G_{3/2}^0$	4	3.30	4.9	4.	97	$g^4F_{9/2}^0$	10	6.34	9.2	0.
48	$z^4F_{9/2}^0$	10	3.51	27.	-2.	98	$g^4F_{7/2}^0$	8	6.35	11.2	0.
49	$z^4F_{7/2}^0$	8	3.57	21.9	1.	99	$g^4F_{5/2}^0$	6	6.46	13.9	0.
50	$z^4F_{5/2}^0$	6	3.62	18.7	1.	100	$g^4F_{3/2}^0$	4	6.53	14.	0.
Co II											
1	a^5P_3	7	2.20	40.0	-20.0	4	$z^5D_4^0$	9	5.74	8.0	10.0
2	a^5P_2	5	2.23	49.9	20.0	5	$z^5D_3^0$	7	5.83	8.0	0.
3	a^5P_1	3	2.27	60.0	2.0	6	$z^5D_2^0$	5	5.89	-30.0	12.0